PHYSICAL REVIEW A **93**, 043855 (2016)

Schemes for generation of isolated attosecond pulses of pure circular polarization

C. Hernández-García,[1,2,*] C. G. Durfee,[1,3] D. D. Hickstein,[1] T. Popmintchev,[1] A. Meier,[3] M. M. Murnane,[1,4] H. C. Kapteyn,[1,4] I. J. Sola,[2] A. Jaron-Becker,[1,4] and A. Becker[1,4]

[1]*JILA, University of Colorado at Boulder, Boulder, Colorado 80309-0440, USA*

[2]*Grupo de Investigación en Aplicaciones del Láser y Fotónica, University of Salamanca, E-37008 Salamanca, Spain*

[3]*Department of Physics, Colorado School of Mines, Golden, Colorado 80401, USA*

[4]*Department of Physics, University of Colorado at Boulder, Boulder, Colorado 80309-0440, USA*

(Received 3 February 2016; published 28 April 2016)

We propose and analyze two schemes capable of generating isolated attosecond pulses of pure circular polarization, based on results of numerical simulations. Both schemes utilize the generation of circularly polarized high-order-harmonics by crossing two circularly polarized counter-rotating pulses in a noncollinear geometry. Our results show that in this setup isolation of a single attosecond pulse can be achieved either by restricting the driver pulse duration to a few cycles or by temporally delaying the two crossed driver pulses. We further propose to compensate the temporal walk-off between the pulses across the focal spot and increasing the conversion efficiency by using angular spatial chirp to provide perfectly matched pulse fronts. The isolation of pure circularly polarized attosecond pulses, along with the opportunity to select their central energy and helicity in the noncollinear technique, opens new perspectives from which to study ultrafast dynamics in chiral systems and magnetic materials.

DOI: 10.1103/PhysRevA.93.043855

I. INTRODUCTION

Capture and control of ultrafast physical processes involving electron dynamics require the development of sources and measurement techniques operating on time scales of the order of attoseconds (1 as $= 10^{-18}$ s) to femtoseconds (1 fs $= 10^{-15}$ s). High-order-harmonic generation (HHG) is an established table-top laboratory light source that produces coherent radiation at extreme ultraviolet (EUV) to soft-x-ray wavelengths in bursts as short as a few tens of attoseconds [1–6]. For many years experimental research in HHG focused on the generation and application of linearly polarized harmonics and attosecond pulses. The physical mechanism at the microscopic level is well understood within the so-called three-step model [7,8]: Following the release of an electron via tunnel ionization from the atom or molecule in an intense laser field, the electron is accelerated by the field and can be driven back to the parent ion. Upon recombination with the ion, the energy is released in the form of high-harmonic radiation.

This HHG technique with a one-color many-cycle linearly polarized driver pulse produces a train of several attosecond bursts [9]. Several schemes to isolate a single linearly polarized attosecond pulse have been developed and successfully implemented, such as reduction of driver pulse duration to a few cycles [10,11], polarization gating schemes [12–14], combination of multicolor fields [15], spatiotemporal focusing [16], and ionization or time-gated phase-matching techniques [17–19].

Despite this substantial progress, the restriction in polarization of available attosecond pulses and pulse trains limits the prospects of ultrafast observations. Although techniques to produce isolated attosecond pulses with elliptical polarization have been proposed [20–23] to the best of our knowledge, so far there does not exist a practical proposal for a table-top laboratory setup generating an isolated attosecond pulse of pure circular polarization. The availability of such pulses would be of importance for a new regime of applications across several areas of physics, ranging from generation of vortex patterns in photoelectron momentum distributions [24], via observation of ultrafast dynamics of photoelectron circular dichroism in chiral molecules [25] to ultrafast imaging of magnetic circular dichroism [26,27]. In this paper we propose, based on results of numerical simulations, two schemes capable of overcoming this obstacle.

Although the physical principle has been proposed and used much earlier [28–30], controlling the polarization of the harmonics has become a center of interest more recently. While different techniques have been used to generate elliptically polarized harmonics [25,31–34], the efficient generation of EUV [26,35] and soft-x-ray [27] beams of pure circular polarization was demonstrated by using bichromatic collinear beams with counter-rotating circular polarization, phase matched in a gas-filled waveguide. Another related technique, using noncollinear, counter-rotating beams [36], provides the additional capability of spatially separating circularly polarized high harmonics of different energy and helicity; however it is so far limited to the EUV region and lower flux.

The proposed schemes for the generation of isolated attosecond pulses of pure circular polarization utilize the noncollinear technique of generating circularly polarized high-order-harmonics [36]. It consists of focusing two crossed counter-rotating pulses into a gas target (Fig. 1). Though the technique does not depend on the specific wavelength of each pulse, here we consider circularly polarized pulses having the same wavelength and equal amplitude. A key element for the proposed isolation schemes is that the superposition of the electric fields of the two beams at the focal plane yields a linearly polarized electric field that rotates as a function of the transverse position (see inset in Fig. 1). Thus, locally at any point in the focus the same single-atom physics as for linearly polarized high-harmonic generation

*carloshergar@usal.es

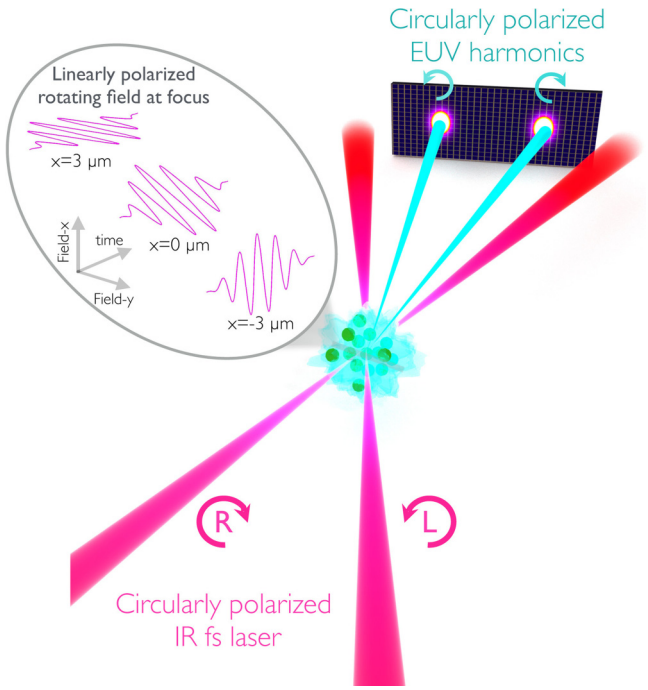

FIG. 1. Scheme of noncollinear circularly polarized, high-harmonic generation (NCP-HHG): Two counter-rotating circularly polarized femtosecond laser pulses are focused into a gas to produce both left and right circularly polarized harmonic beams. At the focal plane, the two circularly polarized beams sum to yield an electric field that exhibits linear polarization, which rotates as a function of the transverse position across the laser focus (inset). The locally linear nature of the polarization enables the application of schemes to isolate a single attosecond pulse, known from linearly polarized harmonic and attosecond pulse generation.

applies. Consequently, strategies, previously established to isolate linearly polarized attosecond pulses, can be adopted to generate isolated circularly polarized HHG pulses in the noncollinear technique. Since furthermore each harmonic order emerges at a different angle and harmonic beams with right and left circular polarization are separated in the far field, the capability of generating isolated attosecond pulses of pure circular polarization comes along with the opportunity of selecting the central energy and helicity of the light field.

The paper is organized as follows: In Sec. II A we study the isolation process provided by restricting the pulse duration of the driver pulses to a single cycle. We feature the significance of the results in the noncollinear geometry by contrasting them to those obtained in the bichromatic collinear geometry (Sec. II B) as well as by demonstrating the opportunities to select helicity and central energy of the isolated pulses (Sec. II C.). In Sec. II D, we show that the efficiency of the noncollinear HHG generation process and, hence, the flux of the isolated attosecond pulses can be increased by introducing angular chirp into the driving beams. In Sec. III, we then analyze a second alternative method, in which a time delay between the pulses provides a polarization gating scheme that enables the generation of isolated circularly polarized pulses even when longer driving laser pulses are used. We end with a brief summary of the results.

II. ISOLATED CIRCULARLY POLARIZED ATTOSECOND PULSES DRIVEN BY SINGLE-CYCLE PULSES

In order to study the generation of high harmonics and attosecond pulses through the NCP-HHG scheme, we perform numerical simulations including propagation through the electromagnetic field propagator [37]. The single-atom dipole acceleration is computed using the SFA+, an extension of the strong-field approximation [38] The gas in the interaction region is modeled as an argon gas at a pressure of 5 Torr. The signal at the detector is computed as the coherent addition of the HHG contributions of all the elementary sources, where the HHG light is assumed to propagate to the detector with a phase velocity equal to the speed of light c and propagation effects of the fundamental field are taken into account.

A. Generation of isolated attosecond pulses of pure circular polarization in a noncollinear geometry

In Fig. 2 we present the attosecond pulses generated by two counter-rotating circularly polarized beams in a noncollinear one-color (left-hand panels) geometry for long (upper row) and ultrashort (lower row) pulses. For the simulations the driving field at the focus is given by the superposition of two beams, E_+ and E_-:

$$\begin{aligned}\mathbf{E}_{\pm}(\mathbf{r},t) &= E_0 A(t) \\ &\times U(x, y\cos\theta_{NC} \mp z\sin\theta_{\rm NC}, \pm y\sin\theta_{\rm NC} + z\cos\theta_{\rm NC}) \\ &\times [\cos(2\pi ct/\lambda + \phi_0)\mathbf{e}_x \pm \sin(2\pi ct/\lambda + \phi_0)\mathbf{e}_y], \end{aligned} \quad (1)$$

where the $\pm$ sign reflects the geometrical and polarization differences between the two noncollinear beams. The wavelength of both beams is chosen to be $\lambda = 800$ nm, with a carrier-envelope phase of $\phi_0 = \pi/4$, and $\theta_{\rm NC} = 32$ mrad is the crossing angle, which is chosen to match typical experimental conditions [36]. Each noncollinear driving beam is assumed to have a Gaussian spatial profile, $U(x',y',z')$, propagating in the z' direction, with a beam waist of 80 μm. The laser pulse envelope $A(t)$ is modeled by a $\sin^2$ function truncated at the first zeros, with a peak intensity of $E_0^2 = 8.75 \times 10^{13}$ W/cm^2 at the focus for each beam and pulse durations of $t_{\rm FWHM} = 5.8$ cycles (15.4 fs, upper panels) and $t_{\rm FWHM} = 1.1$ cycles (2.9 fs, lower panels) full width at half maximum (FWHM) in intensity.

As shown before and observed in the experiments [36], for counter-rotating noncollinear mixing the resulting spectrum [Fig. 2(a)] consists of spatially separated harmonic beams with right and left circular polarization. For the longer driver pulse [Fig. 2(a)] well-separated harmonics can be seen, while for the ultrashort driver pulse [Fig. 2(b)] a more continuous spectrum of harmonic radiation (on a linear scale) is observed. In Figs. 2(c) and 2(d) we present the attosecond wave forms which we obtained by Fourier transformation of the harmonic spectrum detected at 1.7 mrad. For the long driver pulse [Fig. 2(c)] we obtain a pulse train of two circularly polarized pulses per cycle, which in the case of a few-cycle driver pulse [Fig. 2(d)] is confined to an isolated pulse of attosecond radiation of circular polarization (with a couple of small side bursts). The pulse duration of the central burst is 360 as (at intensity FWHM), and the intensities of the side bursts are suppressed to about 2% of the central burst. Thus, as expected

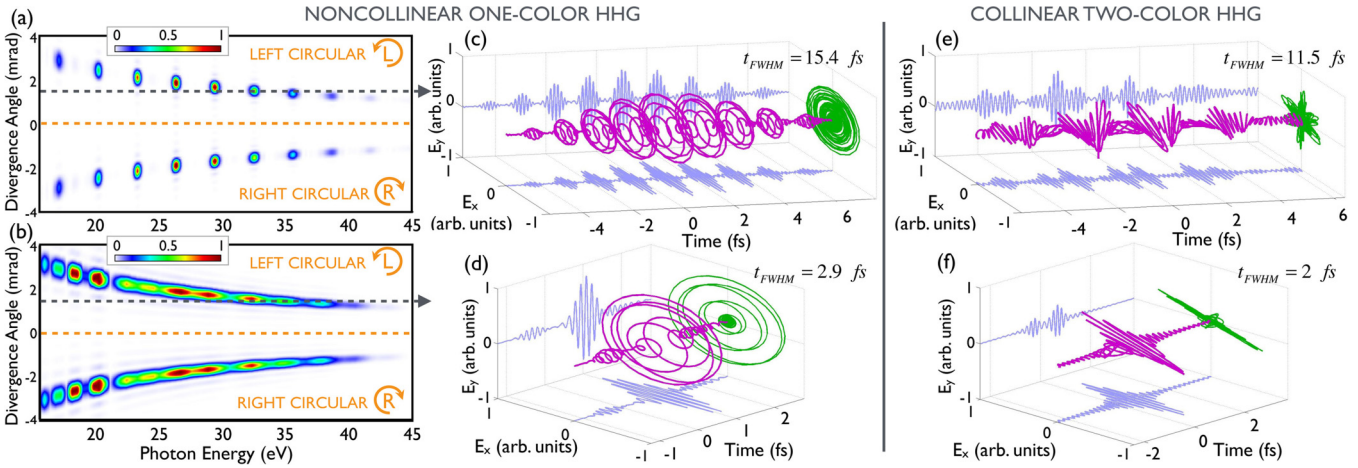

FIG. 2. Comparison of circularly polarized attosecond pulses obtained through NCP-HHG and linearly polarized pulses driven by collinear two-color beams. Results are shown for relatively long (upper row) and ultrashort (lower row) driver pulses. Harmonic spectra [panels (a) and (b)] and circularly polarized attosecond pulses [panels (c) and (d)] for 800-nm counter-rotating noncollinear mixing with $\theta_{NC} = 32$ mrad and laser pulse durations $t_{FWHM} = 5.8$ cycles (15.4 fs) and $t_{FWHM} = 1.1$ cycles (2.9 fs), respectively. Panels (e) and (f) show the linearly polarized attosecond pulses obtained using the collinear bichromatic (800 and 400 nm) scheme, for $t_{FWHM,1} = t_{FWHM,2} = 11.5$-fs driver laser pulses and $t_{FWHM,1} = t_{FWHM,2} = 2$-fs driver laser pulses, respectively.

due to the superposition of the two beams to a local linearly polarized driving field with a rotating polarization direction as a function of the transverse position, attosecond pulses of circular polarization are generated upon each recombination event. Furthermore, as in the case of linearly polarized harmonics [10,11], the reduction of the duration of the driver pulse leads to the isolation of a single burst.

B. Comparison of attosecond pulse generation in collinear and noncollinear geometry

In order to demonstrate the significance of this result obtained in the noncollinear geometry, we use the same strategy for bichromatic collinear beams with counter-rotating circular polarization. As mentioned at the outset, the collinear technique leads to the efficient generation of circularly polarized harmonics beams as well [26,27,35]. However, as we show now, in that geometry the restriction to few-cycle driver pulses leads to the isolation of an attosecond pulse but of linear polarization.

Since our results indicate that in this geometry the isolation of a single burst requires the restriction of the driver pulse length to a regime in which S-matrix theories become unreliable due to nonadiabatic effects [39], we perform single-atom simulations by numerically solving the time-dependent Schrödinger equation in hydrogen, which has an ionization potential similar to that of argon. In the simulations for the collinear bichromatic case the driving field is described as a superposition of two counter-rotating circularly polarized laser pulses in the form of

$$\mathbf{E}_{C,i}(t) = A_i(t)E_{0,i}[\cos(2\pi ct/\lambda_i + \phi_0)\mathbf{e}_x \pm \sin(2\pi ct/\lambda_i + \phi_0)\mathbf{e}_y], \quad (2)$$

where $\lambda_1 = 800$ nm, $\lambda_2 = 400$ nm, $E_{0,1}^2 = E_{0,2}^2 = 8.75 \times 10^{13}$ W/cm^2, and $\phi_0 = \pi/2$. The pulse envelopes $A_i(t)$ are modeled, as in the case of noncollinear beams, via a $\sin^2$ function and the envelope's pulse durations are $t_{FWHM,1} = t_{FWHM,2} = 11.5$ fs [Fig. 2(e)] and $t_{FWHM,1} = t_{FWHM,2} = 2$ fs [Fig. 2(f)].

The attosecond pulses generated in the collinear two-color scheme show different polarization characteristics. As observed in previous works [23,30], the resulting spectrum exhibits two families of alternative counter-rotating circularly polarized harmonics and, hence, the attosecond pulse train consists of three linearly polarized bursts per laser cycle, where the polarization rotates 120° between each burst [Fig. 2(e)]. Consequently, the reduction of the driver pulse duration leads to the isolation of a single pulse [Fig. 2(f)] of linear polarization instead of circular polarization as in the noncollinear scheme.

C. Selection of central energy of the isolated circularly polarized pulse in noncollinear geometry

Beyond the generation and isolation of circularly polarized attosecond pulses, the noncollinear scheme offers another feature, namely, the spatial separation of attosecond pulses at different central energies. In the noncollinear HHG process, different harmonics are emitted with different angles, as shown in Figs. 2(a) and 2(b). As a consequence, it is straightforward to spatially select different parts of the harmonic spectrum.

This can be seen in Fig. 3, which shows the HHG spectrum (first column), time-frequency analysis (second column), and attosecond pulse (third column) obtained at three different divergence angles, 1 mrad (a), 1.5 mrad (b), and 2 mrad (c), corresponding to the simulations presented in Fig. 2(b). Three different spectra centered at 37, 32, and 26 eV are obtained. Note that at each angle different spectral components overlap and, hence, isolated attosecond pulses with different central energies are generated. The overlap of the spectral components at a given detection angle depends on the beam waist of the noncollinear beams and on their crossing angle, θ_{NC}. Smaller crossing angles and larger beam waists would result in broader spectral overlapping. On the other hand, the overlap can also be achieved by refocusing the harmonic light to the target. We

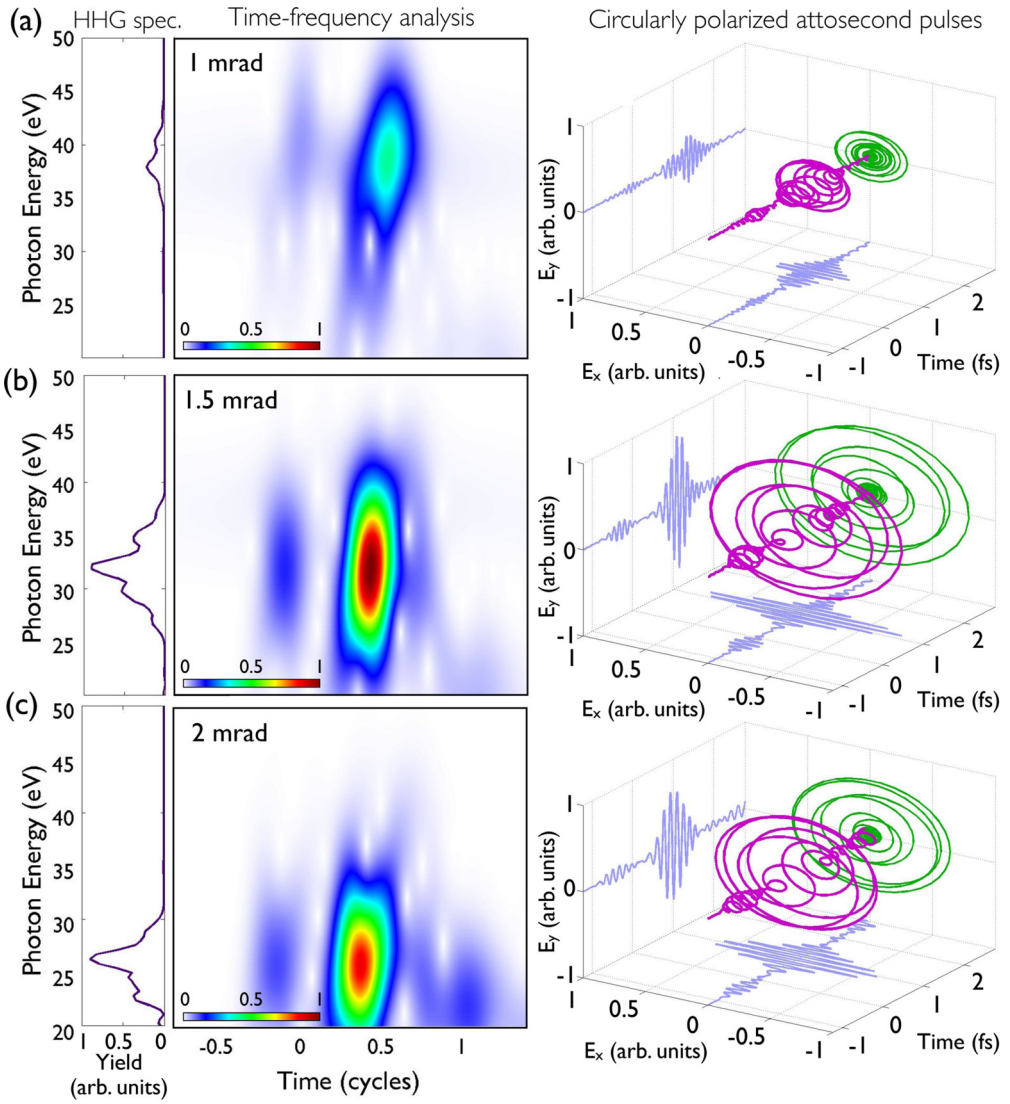

FIG. 3. Spatial selection of isolated circularly polarized attosecond pulses with different frequencies. Shown are the HHG spectrum (first column), time-frequency analysis (second column), and attosecond pulse (third column) obtained at three different divergence angles: 1 mrad (a), 1.5 mrad (b), and 2 mrad (c), corresponding to the results presented in Fig. 2(b).

note that such refocusing may alter the temporal structure of the attosecond pulse from that observed at any given angle (Fig. 3). In this case techniques for the compensation of the spatial chirp may be applicable, if necessary. Numerical studies of such scenarios are beyond the scope of the present analysis, which demonstrates the emission of isolated attosecond pulses with a rather broad spectrum at any given divergence angle in the noncollinear method itself only.

The time-frequency analysis in Fig. 3 (left column) exhibits a structure with positive slope, since the macroscopic addition of the single-atom results favors the so-called short quantum paths in the HHG process. Thus, the circularly polarized attosecond pulses are emitted with a positive chirp, as is the case for HHG driven by a single-cycle linearly polarized pulse [40].

D. Compensation of transverse temporal walk-off with angular chirp

In the noncollinear geometry with conventional focusing, the pulse fronts (i.e., the intensity envelopes) of each beam are not parallel. Therefore, there is a temporal walk-off between each noncollinear laser pulse across the focal spot [see Fig. 4(a)]. At the focal plane, this temporal walk-off is given by

$$\tau_{\mathrm{wo}} = \frac{\sin\theta_{\mathrm{NC}}}{c} x, \tag{3}$$

where x is the transverse position and θ_{NC} is the crossing angle between the two beams. With temporal walk-off, the relative amplitudes of the two fields become a function of time. For two Gaussian pulses of counter-rotating polarization and equal amplitude and pulse duration ($1/e^2$ half-width τ), delayed by $t_d = \tau_{\mathrm{wo}}$, we calculate the time-varying ellipticity of the resulting pulse:

$$\varepsilon(t) = \tanh\left(\frac{2t_d}{\tau^2} t\right). \tag{4}$$

Thus, by superposing the two noncollinear laser pulses at the focal plane, the walk-off delay in the envelopes of each pulse

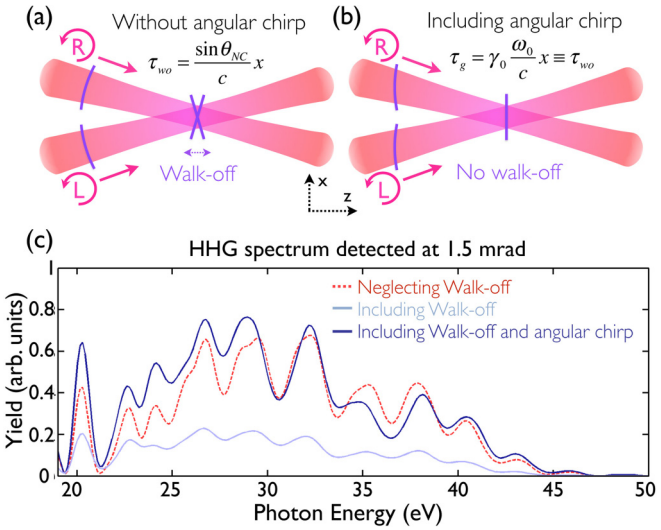

FIG. 4. Compensation of transversal temporal walk-off using angularly chirped noncollinear beams. Shown are schematics of the wave fronts due to the transverse walk-off (a) and after compensation using pulse-front-tilted beams, with opposite angular chirp rate (b). In panel (c) a comparison of the harmonic spectra at 1.5 mrad with (dashed red line) and without (light blue line) transverse walk-off effect, as well as after compensation with angular chirp (dark blue line) are shown. Laser parameters are given in the text.

restricts the spatial region over which polarization is linear. This effect reduces the total HHG yield and the attosecond pulse intensity, since the HHG conversion efficiency drops quickly with increasing ellipticity [41].

In Fig. 4(c) we compare simulated HHG spectra, detected at an angle of 2 mrad, in which the walk-off effect is taken into account (light blue line) and, for the sake of comparison, neglected (dashed red line). The simulation parameters are the same as those in Fig. 2(b), i.e., a laser pulse of $t_{\mathrm{FWHM}} = 2.9$ fs with a crossing angle of $\theta_{\mathrm{NC}} = 32$ mrad, but now with a Gaussian beam radius of 40 μm. We have reduced the beam waist in order to compensate for the increase in computation time due to the higher resolution in the frequency domain needed for this kind of calculations. We can observe that in this case, the temporal walk-off reduces the HHG yield by a factor of 2 to 4 (cf., dashed red and light blue lines). The suppression would further increase with increasing θ_{NC} and/or the beam waist. On the other hand, the effect is smaller for longer pulses.

In order to compensate for the temporal walk-off, we propose to imprint an opposite pulse front tilt in the noncollinear beams via an angular spatial chirp. To this end, we consider beams with transverse spatial chirp, where all the spectral components travel as beamlets in the same direction but with a transverse offset proportional to the frequency offset:

$$x_s(\omega) = \alpha(\omega - \omega_0), \tag{5}$$

where α is the transverse chirp rate. With a lens or curved mirror such a beam with transverse spatial chirp will produce a beam with pure angular chirp at the focal plane [42]. In that case, the beam angle θ_x changes with the frequency in terms of the angular chirp rate γ_0 as

$$\tan\theta_x(\omega - \omega_0) = \gamma_0(\omega - \omega_0), \tag{6}$$

where $\gamma_0 = -\alpha/f$ and f is the lens focal length. This configuration, where the spectral components overlap with an angular sweep, is known as simultaneous space-time focusing [43]. Using the small-angle approximation, $\tan\theta_x \approx \sin\theta_x$, the spectral phase of the pulse at the focal plane can be written as

$$\phi(x,\omega) = \omega \sin\theta_x(\omega) x/c. \tag{7}$$

By calculating the group delay via the first derivative of the phase, we obtain

$$\tau_g = \gamma_0 \frac{\omega_0}{c} x, \tag{8}$$

that is, the group delay varies linearly across the focal spot, exhibiting a pulse front tilt of the beam [42]. The angular spatial chirp, which can be characterized by interferometric techniques [44], has been recently proposed as an element to improve the spectral and temporal resolution of HHG [45].

If the noncollinear beams are sculpted with opposing pulse front tilt so that the intensity envelopes match across the focal spot, perfect temporal overlap between the pulses can be achieved [see Fig. 4(b)]. As a result, the electric field along the transverse direction will exhibit perfect linear polarization. Comparing Eqs. (2) and (8), the spatial chirp rate required for compensating the transverse temporal walk-off is

$$\gamma_0 = \frac{\sin\theta_{\mathrm{NC}}}{\omega_0}. \tag{9}$$

Such an angular dispersion required for pulse front overlap can be achieved by using a diffraction grating as a beam splitter and imaging the grating to the interaction target [46,47].

The dark blue line in Fig. 4(c) shows the HHG spectrum obtained when the transverse walk-off is included and compensated with opposite angular chirp in each of the noncollinear beams. In the corresponding simulations the spatial chirp rate, according to Eq. (9), is $\gamma_0 = 13.56$ as. We indeed observe that the compensation via the angular chirp leads to HHG yields similar to those obtained without the walk-off effect.

III. ISOLATED CIRCULARLY POLARIZED ATTOSECOND PULSES DRIVEN BY TIME-DELAYED LONG PULSES

In Sec. II, we analyzed the generation of isolated circularly polarized attosecond pulses using near-single-cycle driving laser pulses. Those driver pulses are however difficult to obtain in the laboratory. In addition, effects such the transverse temporal walk-off, discussed in Sec. II D, are more effective for short driving pulses. To this end, we have also analyzed schemes to obtain isolated circularly polarized attosecond pulses with longer driving pulses. These schemes can be considered as extensions of the polarization gating technique, which has been successfully applied in linearly polarized HHG to obtain isolated linearly polarized attosecond pulses [12–14]. For example, in Ref. [12] it is shown that two quarter wave plates can be used to produce a few-cycle pulse. In this case the polarization is linear at the center of the pulse only and elliptical at times away from the peak of the pulse. One way to apply this approach in the noncollinear method could be to

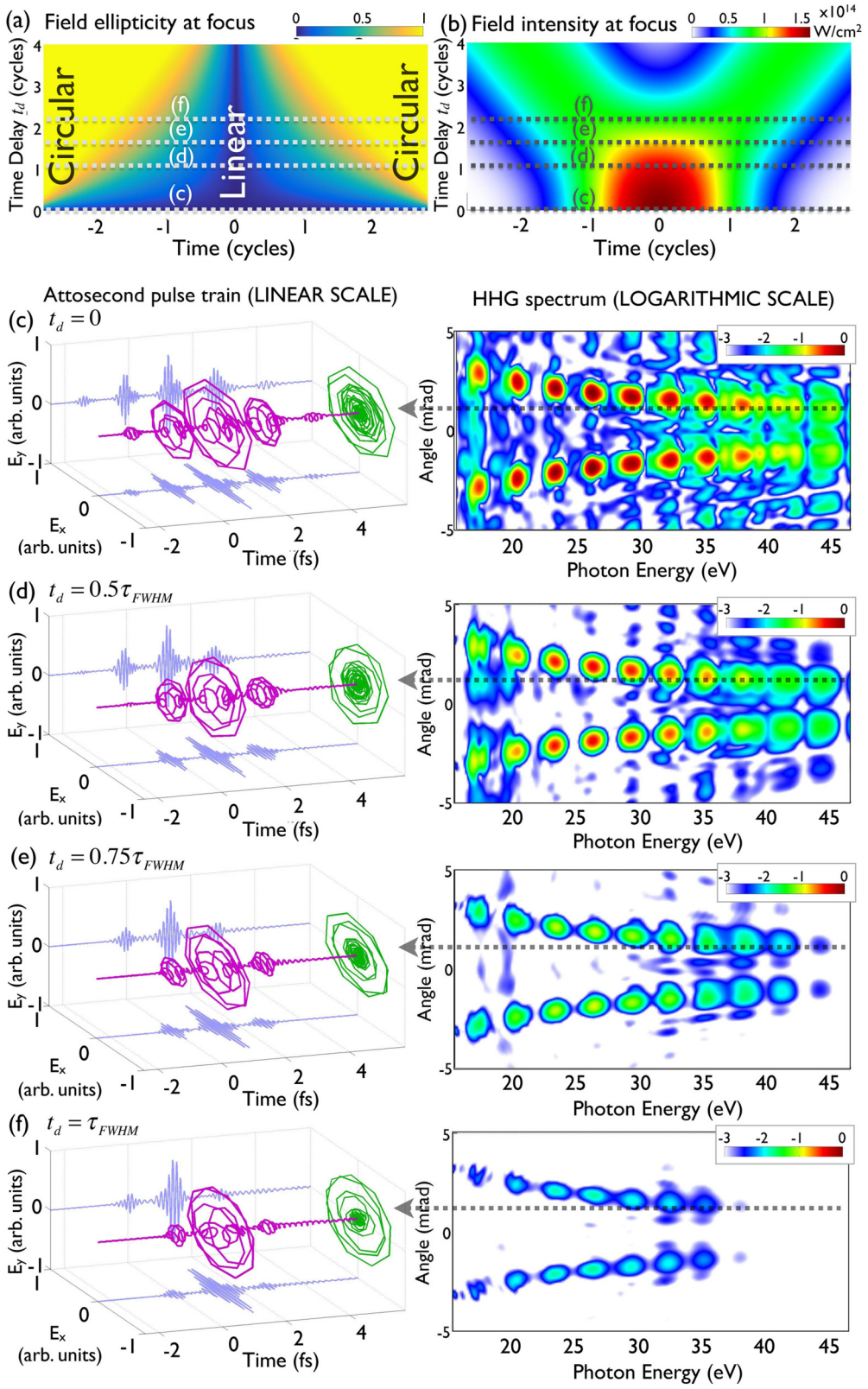

FIG. 5. Time-gating mechanism for generating an isolated circularly polarized attosecond pulse with longer driving pulses. Ellipticity (a) and intensity (b) of the resulting laser pulse at the focus position as a function of the time delay t_d between the two noncollinear pulses. Attosecond pulses (left, linear scale, amplitude normalized to 1 in each panel) and HHG spectra (right, logarithmic scale) obtained in a NCP-HHG scheme for (c) $t_d = 0$, (d) $t_d = 0.5t_{\mathrm{FWHM}}$, (e) $t_d = 0.75t_{\mathrm{FWHM}}$, and (f) $t_d = t_{\mathrm{FWHM}}$. Laser parameters are as in Figs. 2(b) and 2(d), except that the pulse duration is doubled to 5.8 fs.

create a pulse whose polarization is *circular* only at the pulse peak and use this in one or both beams.

A simpler approach, however, is to exploit the effect of a temporal delay t_d between the two noncollinear pulses, which we have discussed in the context of the walk-off delay in Sec. II D. Any delay results in a temporal evolution of the polarization of the resulting pulse at the focal plane [see Eq. (4)]. By deliberately delaying the two pulses to each other, an effective polarization gate can be designed in which the polarization of the resulting pulse changes from circular to linear and back to circular. This is illustrated in Fig. 5, where we present the ellipticity (a) and intensity (b) of the resulting laser pulse at the focus position as a function of the time delay t_d between the two noncollinear pulses. Note that the temporal window over which linear polarization is obtained decreases as the time delay is increased. Since attosecond pulses are emitted more efficiently for linearly polarized drivers, the time-delay between the noncollinear beams gives the opportunity to control the number of attosecond pulses emitted within the train and, therefore, to isolate a single circularly polarized attosecond pulse. However, the intensity at the center of the pulse reduces, as the time delay increases [see Fig. 5(b)], and therefore the cutoff energy of the resulting HHG yield and the efficiency of the yield are expected to be reduced.

In the other panels of Fig. 5 we present the attosecond pulses (linear scale) and HHG spectra (logarithmic scale) obtained using this scheme in the noncollinear geometry, where the pulse duration of the driving pulses is $t_{\mathrm{FWHM}} = 2.2$ cycles (5.8 fs). In order to visualize the gating technique towards the isolation of the central cycle, the attosecond pulses' yields have been normalized in each panel. Note that all laser parameters are the same as those in Figs. 2(b) and 2(d), except the pulse duration, which is doubled. We did not include the transversal walk-off effect in these calculations, as it is expected to be smaller than for the ultrashort pulses studied in the last section and a near-perfect compensation can be achieved.

The results of the simulations indeed confirm that, as the time delay increases from $t_d = 0$ [Fig. 5(c)] to $t_d = t_{\mathrm{FWHM}}$ [Fig. 5(f)], the side bursts in the train get suppressed relative to the main center cycle burst, and, hence, the number of attosecond pulses within the train reduces towards the selection of an isolated circularly polarized attosecond pulse. While the intensities of the adjacent side pulses in Fig. 5(c) ($t_d = 0$) are 42% and 23% of that of the central pulse, in Fig. 5(f) ($t_d = t_{\mathrm{FWHM}}$) they are 3% and 2%, respectively. The pulse duration of the central burst in Fig. 5(f) is 300 as (at intensity FWHM). At the same time, we see that, as expected, the cutoff energy and the harmonic yield are reduced, as compared to the case without any delay. Thus, the isolation of circularly polarized attosecond pulses is indeed possible, even with longer-duration driving lasers, though there is a trade-off in conversion efficiency.

IV. SUMMARY

In summary, we have used the results of numerical simulations to propose and analyze different schemes of generating isolated circularly polarized laser pulses via high harmonic generation with noncollinear counter-rotating driver pulses of the same wavelength. It is shown that the reduction of the driver pulse duration reduces the number of circularly polarized pulses in the attosecond pulse train, similarly to results previously observed in the case of linearly polarized pulses. Due to the emission of each harmonic at a different divergence angle in the noncollinear technique, the central energy of the isolated attosecond pulse and the handedness of the circular polarization can be selected in the far field. The loss of conversion efficiency due to the transversal walk-off in the case of few-cycle pulses can be compensated by matching the pulse front tilt in the noncollinear beams via an angular spatial chirp.

We have further shown that a time-delay between the two noncollinear pulses generates an effective polarization gate in the resulting pulse at the focal plane. This provides an alternative route to the generation of isolated circularly polarized attosecond pulses even with longer-duration driving pulses. This time-gating method for isolating attosecond pulses is anticipated to be more effective for longer-wavelength driving pulses since in this case HHG is more sensitive to the ellipticity of the driver pulse.

ACKNOWLEDGMENTS

The authors acknowledge Luis Plaja for valuable discussions. C.H.-G. acknowledges support from the Marie Curie International Outgoing Fellowship within the EU Seventh Framework Programme for Research and Technological Development (2007–2013), under REA Grant Agreement No. 328334. C.H.-G. and I.J.S. acknowledge support from Junta de Castilla y León (Project SA116U13, UIC016) and MINECO (Grants No. FIS2013-44174-P and No. FIS2015-71933-REDT). A.J.-B. was supported by grants from the U.S. National Science Foundation (Grants No. PHY-1125844 and No. PHY-1068706). D.H. was supported via a grant from the Department of Energy. M.M.M., H.C.K., C.G.D., and A.B. acknowledge support by a MURI grant from Air Force Office of Scientific Research under Award Number FA9550-16-1-0121. This work utilized the Janus supercomputer, which is supported by the U.S. National Science Foundation (Grant No. CNS-0821794) and the University of Colorado Boulder.

[1] P. Agostini and L. F. DiMauro, Rep. Prog. Phys. **67**, 813 (2004).
[2] P. B. Corkum and F. Krausz, Nat. Phys. **3**, 381 (2007).
[3] M. B. Gaarde, J. L. Tate, and K. J. Schafer, J. Phys. B **41**, 132001 (2008).
[4] F. Krausz and M. Ivanov, Rev. Mod. Phys. **81**, 163 (2009).
[5] T. Popmintchev, M. C. Chen, P. Arpin, M. M. Murnane, and H. C. Kapteyn, Nat. Photonics **4**, 822 (2010).
[6] J. Miao, T. Ishikawa, I. K. Robinson, and M. M. Murnane, Science **348**, 530 (2015).
[7] K. J. Schafer, B. Yang, L. F. DiMauro, and K. C. Kulander, Phys. Rev. Lett. **70**, 1599 (1993).

[8] P. B. Corkum, Phys. Rev. Lett. **71**, 1994 (1993).
[9] P. M. Paul, E. S. Toma, P. Breger, G. Mullot, F. Augé, Ph. Balcou, H. G. Muller, and P. Agostini, Science **292**, 1689 (2001).
[10] I. P. Christov, M. M. Murnane, and H. C. Kapteyn, Phys. Rev. Lett. **78**, 1251 (1997).
[11] E. Goulielmakis, M. Schultze, M. Hofstetter, V. S. Yakovlev, J. Gagnon, M. Uiberacker, A. L. Aquila, E. M. Gullikson, D. T. Attwood, R. Kienberger, F. Krausz, and U. Kleineberg, Science **320**, 1614 (2008).
[12] I. J. Sola, E. Mével, L. Elouga, E. Constant, V. Strelkov, L. Poletto, P. Villoresi, E. Benedetti, J.-P. Caumes, S. Stagira, C. Vozzi, G. Sansone, and M. Nisoli, Nat. Phys. **2**, 319 (2006).
[13] G. Sansone, E. Benedetti, F. Calegari, C. Vozzi, L. Avaldi, R. Flammini, L. Poletto, P. Villoresi, C. Altucci, R. Velotta, S. Stagira, S. De Silvestri, and M. Nisoli, Science **314**, 443 (2006).
[14] K. Zhao, Q. Zhang, M. Chini, Y. Wu, X. Wang, and Z. Chang, Opt. Lett. **37**, 3891 (2012).
[15] E. J. Takahashi, P. Lan, O. D. Mücke, Y. Nabekawa, and K. Midorikawa, Phys. Rev. Lett. **104**, 233901 (2010).
[16] H. Vincenti and F. Quéré, Phys. Rev. Lett. **108**, 113904 (2012).
[17] A. S. Sandhu, E. Gagnon, A. Paul, I. Thomann, A. Lytle, T. Keep, M. M. Murnane, H. C. Kapteyn, and I. P. Christov, Phys. Rev. A **74**, 061803R (2006).
[18] M. J. Abel, T. Pfeifer, P. M. Nagel, W. Boutu, M. J. Bell, C. P. Steiner, D. M. Neumark, and S. R. Leone, Chem. Phys. **366**, 9 (2009).
[19] M.-C. Chen, C. Mancuso, C. Hernández-García, F. Dollar, B. Galloway, D. Popmintchev, P. C. Huang, B. Walker, L. Plaja, A. A. Jaroń-Becker, A. Becker, M. M. Murnane, H. C. Kapteyn, and T. Popmintchev, Proc. Natl. Acad. Sci. USA **111**, E2361 (2014).
[20] C. Ruiz, D. J. Hoffmann, R. Torres, L. E. Chipperfield, and J. P. Marangos, New. J. Phys. **11**, 113045 (2009).
[21] D. B. Milosevic, Opt. Lett. **40**, 2381 (2015).
[22] L. Medisauskas, J. Wragg, H. van der Hart, and M. Yu. Ivanov, Phys. Rev. Lett. **115**, 153001 (2015).
[23] C. Chen, Z. Tao, C. Hernández-García, P. Matyba, A. Carr, R. Knut, O. Kfir, D. Zusin, C. Gentry, P. Grychtol, O. Cohen, L. Plaja, A. Becker, A. Jaron-Becker, H. Kapteyn, and M. Murnane, Sci. Adv. **2**, e1501333 (2016).
[24] J. M. Ngoko Djiokap, S. X. Hu, L. B. Madsen, N. L. Manakov, A. V. Meremianin, and A. F. Starace, Phys. Rev. Lett. **115**, 113004 (2015).
[25] A. Ferré, C. Handschin, M. Dumergue, F. Burgy, A. Comby, D. Descamps, B. Fabre, G. A. Garcia, R. Géneaux, L. Merceron, E. Mével, L. Nahon, S. Petit, B. Pons, D. Staedter, S. Weber, T. Ruchon, V. Blanchet, and Y. Mairesse, Nat. Photonics **9**, 93 (2014).
[26] O. Kfir, P. Grychtol, E. Turgut, R. Knut, D. Zusin, D. Popmintchev, T. Popmintchev, H. Nembach, J. M. Shaw, A. Fleischer, H. Kapteyn, M. Murnane, and O. Cohen, Nat. Photon. **9**, 99 (2015).
[27] T. Fan *et al.*, Proc. Natl. Acad. Sci. USA **112**, 14206 (2015).
[28] H. Eichmann, A. Egbert, S. Nolte, C. Momma, B. Wellegehausen, W. Becker, S. Long, and J. K. McIver, Phys. Rev. A **51**, R3414 (1995).
[29] D. B. Milosevic and W. Becker, Phys. Rev. A **62**, 011403(R) (2000).
[30] D. B. Milosevic, W. Becker, and R. Kopold, Phys. Rev. A **61**, 063403 (2000).
[31] X. Zhou, R. Lock, N. Wagner, W. Li, H. C. Kapteyn, and M. M. Murnane, Phys. Rev. Lett. **102**, 073902 (2009).
[32] K. J. Yuan and A. D. Bandrauk, Phys. Rev. A **83**, 063422 (2011).
[33] K. J. Yuan and A. D. Bandrauk, Phys. Rev. A **84**, 023410 (2011).
[34] G. Lambert *et al.*, Nat. Commun. **6**, 6167 (2015).
[35] A. Fleischer, O. Kfir, T. Diskin, P. Sidorenko, and O. Cohen, Nat. Photonics **8**, 543 (2014).
[36] D. D. Hickstein, F. J. Dollar, P. Grychtol, J. L. Ellis, R. Knut, C. Hernández-García, C. Gentry, D. Zusin, J. M. Shaw, T. Fan, K. M. Dorney, A. Becker, A. Jaroń-Becker, H. C. Kapteyn, M. M. Murnane, and Ch. G. Durfee, Nat. Photonics **9**, 743 (2015).
[37] C. Hernández-García, J. A. Pérez-Hernández, J. Ramos, E. C. Jarque, L. Roso, and L. Plaja, Phys. Rev. A **82**, 033432 (2010).
[38] J. A. Pérez-Hernández, L. Roso, and L. Plaja, Opt. Express **17**, 9891 (2009).
[39] A. Becker, L. Plaja, P. Moreno, M. Nurhuda, and F. H. M. Faisal, Phys. Rev. A **64**, 023408 (2001).
[40] Y. Mairesse, A. de Bohan, L. J. Frasinski, H. Merdji, L. C. Dinu, P. Monchicourt, P. Breger, M. Kovacev, R. Taïeb, B. Carré, H. G. Muller, P. Agostini, and P. Salieres, Science **302**, 1540 (2003).
[41] P. Dietrich, N. H. Burnett, M. Ivanov, and P. B. Corkum, Phys. Rev. A **50**, R3585 (1994).
[42] C. G. Durfee, M. Greco, E. Block, D. Vitek, and J. A. Squier, Opt. Express **20**, 14244 (2012).
[43] G. Zhu, J. van Howe, M. Durst, W. Zipfel, and C. Xu, Opt. Express **13**, 2153 (2005).
[44] A. Meier, M. Iliev, J. Squier, and C. Durfee, Opt. Lett. **40**, 4066 (2015).
[45] C. Hernández-García, A. Jaron-Becker, D. D. Hickstein, A. Becker, and C. G. Durfee, Phys. Rev. A **93**, 023825 (2016).
[46] A. Maznev, T. Crimmins, and K. Nelson, Opt. Lett. **23**, 1378 (1998).
[47] A. Meier, Ph.D. Thesis, Colorado School of Mines, Golden, CO, 2015.